GEOPERSIA

Accepted Manuscript

Seismic reflection imaging of an offshore major strike-slip zone and its role in the structural development of western Makran

Mehrdad Sarhangi, Ali Solgi, Morteza Talebian, Zahra Maleki

DOI: 10.22059/geope.2026.406353.648852

Receive Date: 01 December 2025
Revise Date: 27 February 2026
Accept Date: 10 May 2026

Seismic reflection imaging of an offshore major strike-slip zone and its role in the structural development of western Makran

Mehrdad Sarhangi [1], Ali Solgi [1], *, Morteza Talebian [2], Zahra Maleki [1]

[1] Department of Earth Sciences, SR.C., Islamic Azad University, Tehran, Iran
[2] Department of Geology, research Institute for Earth Sciences, Geological Survey of Iran, Tehran, Iran

Received: 01 December 2025, Revised: 27 February 2026, Accepted: 10 May 2026

Abstract
The Zendan–Minab Fault System (ZMFS) forms a major right-lateral shear zone at the transition between the Zagros collision belt and the Makran subduction system. Although its onshore kinematics are relatively well constrained, the geometry and structural role of its offshore continuation in the western Makran remain insufficiently understood. This study investigates the offshore expression of the ZMFS using a regional 4 × 4 km grid of 2D seismic reflection profiles acquired by the National Iranian Oil Company (NIOC) and six depth-migrated seismic sections. Edge-detection techniques were employed to overcome uncertainties arising from the absence of 3D seismic coverage, limited well control, and lower resolution of deeper seismic sections. Most faults in the offshore ZMFS appear geometrically parallel and discontinuous, consistent with soft-linked behavior, and no continuous through-going flower structures can be confidently resolved given the 4 km line spacing; thus, the observed segmentation may partly reflect spatial resolution limitations. GPS-derived rates (~16 mm yr^{-1}) indicate significant offshore strain accumulation along the Zagros–Makran transfer zone, including the ZMFS segment, suggesting that moderate to large earthquakes could occur at intersections of strike-slip and thrust faults, with potential tsunamigenic implications. These observations support interpretation of the offshore ZMFS as a broad transpressional transfer zone accommodating oblique Arabia–Eurasia convergence.

Keywords: Western Makran; Zendan–Minab Fault System; Offshore Strike-Slip Faulting; Accretionary Prism; Transpressional Deformation; Seismic Attribute Analysis.

Introduction

The Zendan–Minab Fault System (ZMFS) (Bayer et al., 2006) is a major right-lateral shear zone located within the transitional domain between the Zagros orogenic belt and the Makran subduction system (Fig. 1). This tectonic boundary accommodates the change from continental collision in the Zagros Fold–Thrust Belt (with high tectonic activities in the crush zone (Aram and Arian,2016) to oceanic subduction in the Oman Sea and is commonly referred to as the Oman Line (Kadinsky-Cade and Barazangi, 1982). To the north, this transition zone is limited by structures related to the Neo-Tethyan suture represented by the Main Zagros Thrust (Ricou, 1977), whereas toward the east it is expressed as a dextral transpressional fault system (Walker and Jackson, 2002; Regard et al., 2010). Rock assemblages exposed along the ZMFS include flysch-type sedimentary successions, ophiolitic fragments, and mélanges (McCall et al., 1994), as a transfer zone linking deformation in the Zagros collision belt with the Makran subduction system (Bayer et al., 2006; Walker and Jackson, 2002; Regard et al., 2010).

* Corresponding author e-mail: Alisolgi@iau.ac.ir

Western Makran is characterized by a lower level of seismic activity compared with eastern Makran, a pattern that cannot be explained by limited instrumental coverage but instead reflects reduced regional strain rates (Abbassi et al., 2023; Akbarzadeh et al., 2023). Geodetic observations confirm that deformation is ongoing along the onshore segment of the ZMFS, with GPS measurements (Fig. 1) indicating accumulation of right-lateral strain (Bayer et al., 2006; Peyret et al., 2009; Penney et al., 2017). More recent analyses suggest enhanced dextral motion across the Zagros–Makran transfer zone (approximately 16 mm/yr) together with pronounced along-strike variations in coupling and strain rate (Abbassi et al., 2023). Seismic tomography based on ambient noise and earthquake surface waves further constrains the crustal and uppermost mantle structure beneath the Iranian Makran and provides insight into factors influencing regional deformation patterns (Ghods et al., 2025). Although these studies significantly improve knowledge of the onshore ZMFS, the geometry and kinematics of its offshore continuation remain poorly constrained.

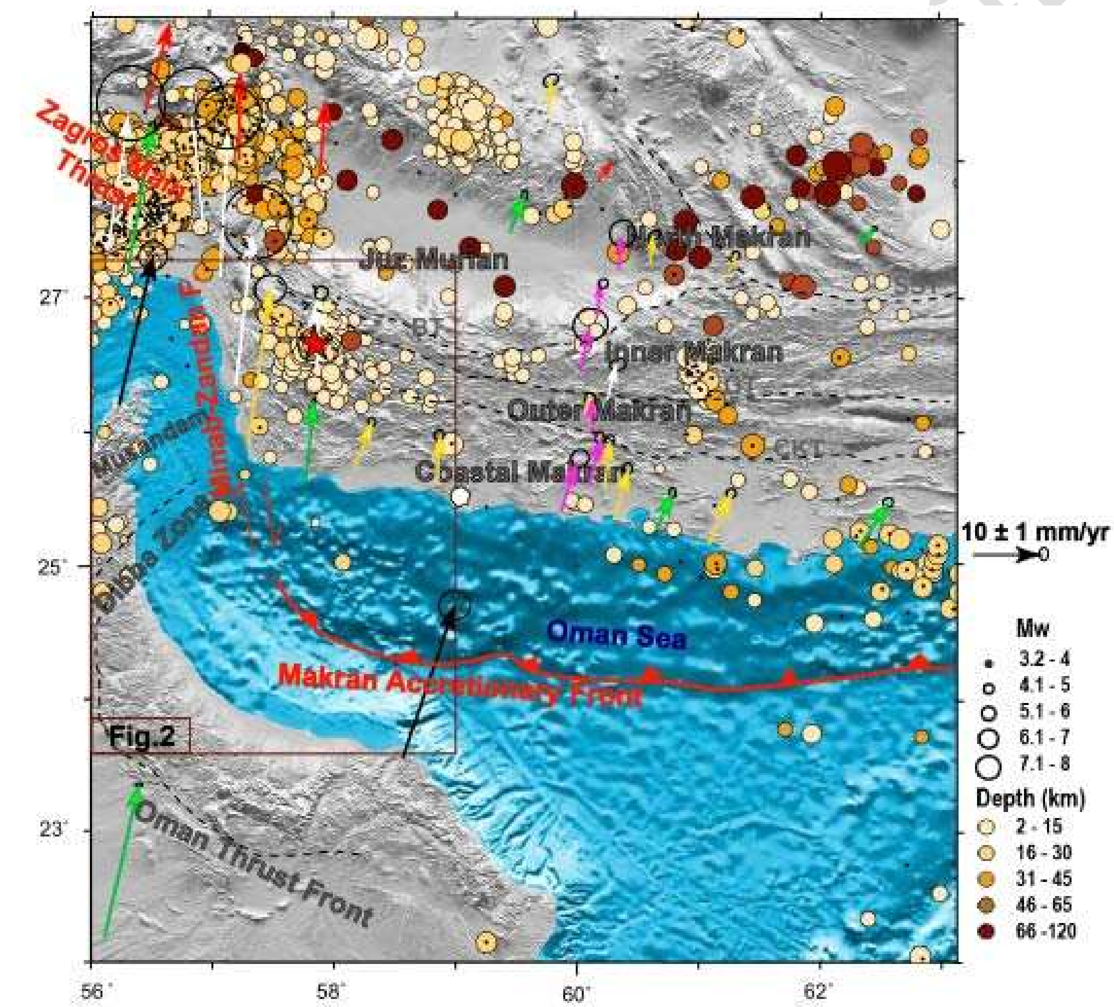

Figure 1. Geodynamic setting of the Zagros–Makran transition zone. Seismicity (earthquakes with magnitude >3.5 since 1945) is shown as colored circles. CKT – Chah Khan Thrust; BT – Bashagard Thrust; GT – Ghasre Ghand Thrust; SST – Sistan Siahan Thrust. A zoomed view of the onshore region is presented in Figure 2. Arrows indicate tectonic plate motions relative to stable Eurasia. GPS velocity vectors, with 95% confidence ellipses, are compiled from Masson et al. (2007), Fröhling and Szeliga (2016), Khorrami et al. (2019), and Abbassi et al. (2023). The red star marks the hypocenter of the 2013 Mw 6.1 earthquake, and the white hexagon denotes the location of the only onshore well

Previous seismic studies identified the southern extension of the ZMFS into the Oman Sea (Ravaut et al., 1998), and recent work (Pajang et al., 2021, 2022) has described offshore structures related to mud volcanism and thrust–normal fault interactions. Offshore, the structural expression of the ZMFS has largely been inferred from map-view interpretations (e.g., Zalan, 1987) and analogs from strike-slip tectonics (Moody and Hill, 1956; Harding, 1985; McClay and Bonora, 2001). In cross-sectional views, strike-slip faults are identified by linear fault traces, en-echelon offsets, and variable displacement along faults (Harding, 1974; Harding, 1985; Harding, 1990; Christie-Blick and Biddle, 1985; Woodcock and Rickards, 2003; Swanson, 2005; Ramadan et al., 2014). Nevertheless, the offshore geometry and kinematics of the ZMFS remain poorly constrained due to the lack of direct subsurface observations. In particular, the style of faulting associated with the offshore continuation of the ZMFS and its interaction with overlying sedimentary structures are not well understood. This study integrates 2D seismic reflection profiles with onshore GPS velocity data and previously reported seismicity to characterize the offshore expression of the ZMFS and to assess its structural relationship with deformation in the western Makran accretionary prism.

Tectonic Setting

The Makran accretionary prism, extending ~900 km along strike (Khaledzadeh et al., 2021), and ~400 km across, with two-thirds exposed onshore, is one of the largest accretionary wedges worldwide (Fig. 1). It forms due to the ongoing subduction of the Arabian Plate beneath the Eurasian Plate, initiated in the Early Cretaceous. Convergence rates vary from ~35–36 mm yr^{-1} in the western Makran to ~39 mm yr^{-1} in the east (Vernant et al., 2004). The subducting slab dips gently (~2–18°) beneath western Makran and more steeply (~8–20°) toward the east, increasing at depth to ~45° beyond 80 km (Kopp et al., 2000; Kukowski et al., 2001; Priestley et al., 2022; Namdarsehat et al., 2024; Ghods et al., 2025). Variations along strike and depth highlight the segmented nature of the subduction zone, which influences seismic potential and strain distribution along the ZMFS.

The Makran prism is classically divided into onshore and offshore domains, separated by the coastal area (Fig. 1). Coastal and offshore areas host normal faults and mud volcanoes (Kukowski et al., 2001; Schlüter et al., 2002; Grando & McClay, 2007; Pajang et al., 2021, 2022), with high sedimentation rates attributed to large fluvial systems draining the Zagros and adjacent regions, supplying clastic material to the Makran basin (Mohammadi et al., 2016, 2017). Submarine olistostromes of Tortonian age indicate that the wedge remained largely submerged until ~12–9 Ma (Burg et al., 2008; Ruh et al., 2018). Offshore seismic profiles reveal structural segmentation: (1) north-dipping imbricated thrusts zone at the front, (2) a diapiric zone of shallow origin, and (3) active listric normal faults rooted in the décollement near the coast (Pajang et al., 2021). The profile 3 of recent tomographic models by Haberland et al. (2020) follows the orange seismic profile shown in Fig.2, extending onshore. It indicates a thick (>10 km) low seismic P-wave velocity (Vp) sedimentary pile beneath the coastal area, consistent with the presence of deep sedimentary basins. The Zagros Orogen, part of the Alpine–Himalayan belt, results from the closure of the southern Neotethys Ocean during the Mesozoic and early Cenozoic (Chiu et al., 2013; Alavi, 1994; Talbot and Alavi, 1996; Casini et al., 2011) and the collision between the Central Iran and Arabian Plates from the late Eocene, (e.g., Hessami et al., 2001; Allen and Armstrong, 2008), to the mid-late Miocene, e.g., (Stoneley, 1981; McQuarrie et al., 2003). GPS measurements indicate N–S shortening rates increasing from ~4 mm yr^{-1} in NW Zagros to ~9 mm yr^{-1} in SE (Vernant et al., 2004; Walpersdorf et al., 2006), with a jump to ~20 mm yr^{-1} at coastal GPS sites located above the Makran subduction interface, implying ~10–13 mm yr^{-1} right-lateral motion across the Zagros–Makran transfer zone (Peyret et al., 2009). Abbassi et al. (2023) suggest a larger strike-slip motion rate of approximately 16 mm yr^{-1} along this transition zone, indicating higher present-day deformation than previously estimated. This zone, including the ZMFS, accommodates strain transferred from the Zagros collision into the Makran wedge (Regard et al., 2004, 2005; Bayer et al., 2006; Peyret et al., 2009; Abbassi et al., 2023).

Part of the ZMFS is located onshore, where en-echelon fault structures are formed by a series of nearly parallel N-S trending right-lateral transpressional faults (Mokhtari et al., 2008). The drag-folds along the main structures on the satellite image infer the right-lateral nature of this fault system (Mokhtari et al., 2008; Regard et al., 2008, 2009, 2010). Toward the east, the fault trace progressively rotates from a dominant N–S trend to a more E–W orientation consistent with the regional Makran structural grain (Burberry and Jackson, 2013; Regard et al., 2009), and locally cross-cuts thrust faults. East of the main fault, lineaments represent younger lateral movements along the southern shoreline, indicating an eastward migration of the fault complex over time. A few studies (Burberry and Jackson, 2013; Ravaut et al., 1998) have briefly shown offshore continuation of ZMFS. Burberry and Jackson (2013) showed a 40 km wide zone of several N-S trending compressional oblique-slip faults with thrust and strike-slip components, which have a more thrust nature closer to the accretionary front. They indicate the N-S trend of the oblique-slip structures has more impact on the deformation pattern. However, the geometry and offshore continuity of the ZMFS, as well as its structural role within the western Makran wedge, remain poorly constrained.

Seismicity and geophysical observations highlight ongoing activity along the ZMFS (Bayer et al. 2006; Peyret et al. 2009; Abbassi et al. 2023). Penney et al. (2017) estimate the interseismic coupling and assume the decrease in velocity towards the coast of Oman is evidence of strain accumulation. However, Regard et al. (2005, 2004) suggest that the total strain accommodated by the ZMFS should decrease from north to south. Microearthquake studies show mixed thrust and right-lateral slip north of the fault (Yamini Fard et al., 2003), consistent with the dominant N–S trend of the ZMFS in its onshore segment. In contrast, the 2013 Mw 6.1 Minab earthquake ruptured an E–W left-lateral strike-slip fault located ~200 km east of the main ZMFS trace, within the Makran domain, and is therefore more likely related to underthrusting of the Arabian lithosphere and regional shear rather than direct rupture of the ZMFS (Penney et al., 2015). Interseismic coupling models and GPS vectors indicate the ZMFS continues to accumulate elastic strain (Bayer et al., 2006; Abbassi et al., 2023; Penney et al., 2017).

Overall, the ZMFS represents the key transition between the Zagros collision zone and the Makran subduction system. Lateral and depth variations in slab geometry, coupled with fault segmentation and ongoing strain accumulation, control seismic hazard and deformation patterns in the region (Bayer et al., 2006; Walker and Jackson, 2002; Regard et al., 2010).

Data and Methodology

Strike-slip tectonics is most commonly analyzed in horizontal sections (map view) (e.g., Zalan, 1987) and less frequently in vertical sections (eg., seismic lines). In map view, strike-slip systems are recognized by features such as linear fault traces, en-échelon arrays, pull-apart basins, and horsetail splays (Moody and Hill, 1956; Harding, 1985; McClay and Bonora, 2001). In cross-sectional seismic profiles, diagnostic features include steep to vertical fault planes, flower structures, abrupt changes in sediment thickness within the same stratigraphic unit, and variable displacement along faults (Harding, 1974; Christie-Blick and Biddle, 1985; Harding, 1990; Woodcock and Rickards, 2003; Swanson, 2005; Ramadan et al., 2014). However, the use of conventional 2D seismic reflection data to determine the continuation and geometry of strike-slip faults remains challenging.

The study area is located in the western Oman Sea and is covered by 2D seismic reflection data acquired during the Persian Carpet 2000 (PC-2000) project. Acquisition was carried out in several phases (NIOC internal report, (Skarpnes et al., 2003)): Phase 1–2: recorded by the seismic vessel Bin Hai 517, with 8192 ms record length, 6000 m streamer, and nominal fold of 120; sources were Bolt airguns (2842 cu in). Data were processed by CGG (Phase 1) and Spectrum (Phase 2). Phase 3: recorded by the vessel *Pejwak*, with a 20480 ms record length, 7200 m streamer, and nominal fold of 90, using a Bolt Long Life source (4436 cu in). Processing was performed by Spectrum.

Overall, the seismic grid covers the study area with a dip- and strike-oriented spacing of 4 × 4 km (Fig. 2a), most of which were recorded with a 6-second record length. Data quality is good in the shallower parts but decreases with depth, particularly below the Upper Miocene sequences (yellow reflector in Fig. 2c).

Velocity control was provided by stacking velocities from each acquisition phase. While velocity trends are consistent to ~4500 ms, deeper intervals exhibit differences between phases due to variations in acquisition and processing. These stacking velocities were used as the primary source for depth conversion.

The study area in the Oman Sea is a frontier area with no wells or proven stratigraphic columns. Only one well was drilled onshore, which reached Upper Miocene sediments composed of silty shales and shaly sands interbedded with thin sandstone intervals (according to the unpublished well report from NIOC).

Offshore wells were drilled in the Pakistani side of the Oman Sea, and some general stratigraphy has been published from onshore Pakistan (Ahmed, 1969; Harms et al., 1984; Ellouz-Zimmermann et al., 2007). However, their correlation cannot be used due to large lateral structural and lithological variations in the Iranian side. Instead in NIOC report, approximate stratigraphic control was obtained by correlating PC-2000 seismic to older NIOC data in the Strait of Hormuz, where two wells (red stars, Fig. 2a) provide limited ties. From these, NIOC determined the H4 horizon (Fig.3) corresponds approximately to the Top Mishan.

Seismic interpretation was carried out by NIOC in order to produce structure maps and delineate regional tectonic provinces. Given the regional grid and complex tectonic overprinting, no detailed seismic facies analysis was attempted. Horizons were picked primarily on the basis of clear unconformities, strong continuous reflectors, and diagnostic features such as the décollement and BSR. Because of lateral variations in basin architecture, several deeper horizons could be traced only locally, and correlation across transfer faults, thrusts (Grando and McClay, 2007; Smith et al., 2012), or mud diapirs was uncertain.

To better illustrate the structure of the area, we present a set of seismic sections oriented west–east and north–south across the study area. A total of eight seismic lines were used in this study, with five oriented approximately east–west and three oriented approximately north–south (Fig. 2a). N–S oriented profiles mainly image thrust-related structures, whereas E–W oriented profiles are more suitable for identifying strike-slip faults and associated lateral offsets along the ZMF. For this study, we adopted the six key horizons identified by NIOC (including the seabed) (Fig. 3) and further screened them across profiles to ensure consistent picking. Each horizon was characterized by distinctive seismic attributes (amplitude, continuity, frequency). We avoided deeper reflectors due to poor resolution and greater interpretational uncertainty.

Because 3D seismic data and offshore wells are lacking, the identification of strike-slip faults relies entirely on 2D seismic profiles, depth-converted maps, and isochore mapping. Horizon interpretation and mapping were carried out in Petrel software. Depth conversion used stack velocity models provided by NIOC, the only available velocity control in the area. The resulting time- and depth-structure maps and isochore maps provided the main basis for fault identification. Potential fault traces corresponding to the ZMFS were digitized in 2D window at multiple stratigraphic levels and then projected into 3D window to evaluate continuity and geometric relationships.

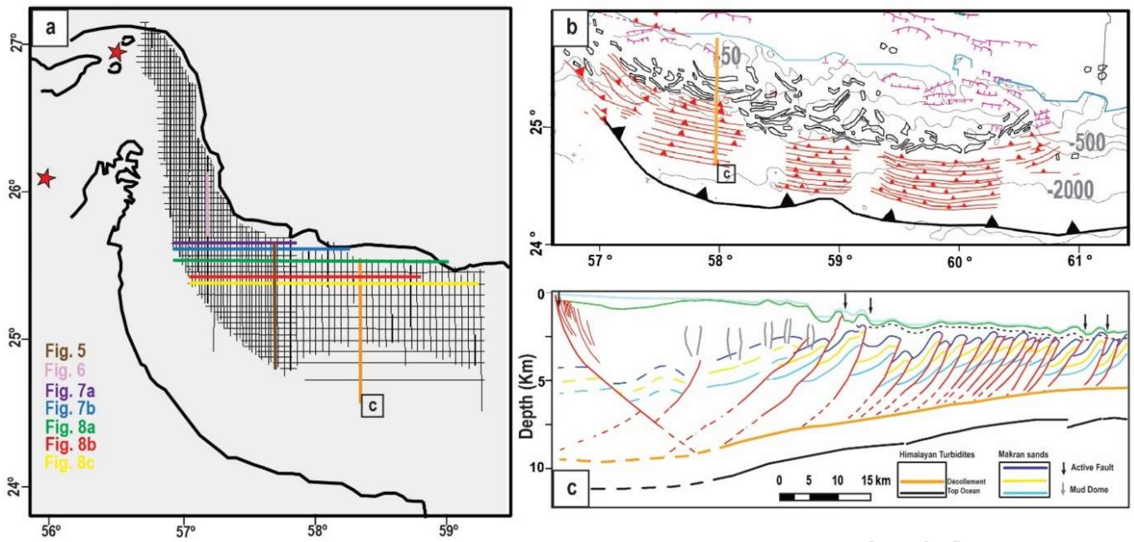

Figure 2. (a) The seismic grid is 4x4 km in the western Oman Sea. The red stars indicate the locations of the wells in the Strait of Hormuz. (b) The offshore structural map, illustrating three different structural domains of the Oman Sea (modified from Pajang et al., 2021). (c) Depth-migrated interpretation of the western cross-section (after Pajang et al., 2021), showing a listric normal fault near the coastline, an imbricated thrust zone toward the deformation front, and a mud volcano belt in between. The orange line in a indicates the location of the cross-section

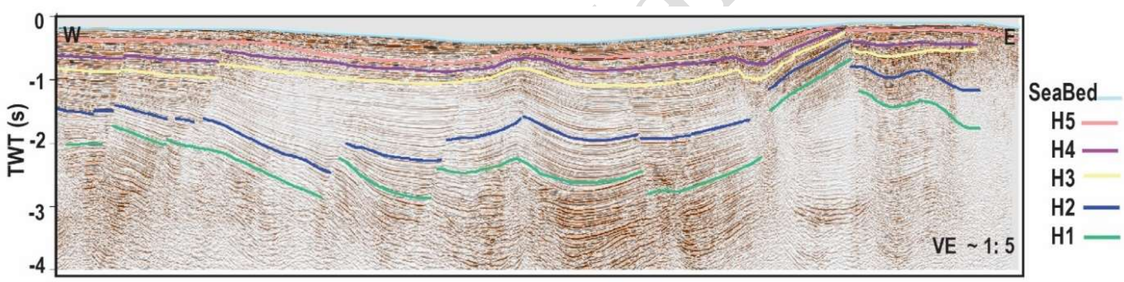

Figure 3. Horizon interpretation used in this study by the names Seabed, H5 to H1. The violet line in Figure 2a indicates its location along west of Oman sea. The line without interpretation is shown in Fig. 6a

Results

Seismic Horizons

We named six seismic horizons reflectors including the seafloor (Seabed) as H1–H5 (Fig. 3). Due to the absence of well data, the ages of these reflectors remain uncertain, but relative stratigraphic assignments are suggested based on NIOC reports. Two unconformities are recognizable as a regionally traceable shallow unconformity (H5), assigned to the Pliocene–Pleistocene and a deeper angular unconformity separating Mid-Miocene sediments from older Eocene–Cretaceous strata (H1). Intermediate reflectors (H2–H4) are regionally continuous and likely represent Pliocene to Middle Miocene successions. These markers provide the framework for structural and stratigraphic mapping.

Structural Trends Onshore and Offshore

The general structural trend of the Makran accretionary prism is E-W, perpendicular to the subduction direction. As we approach the Strait of Hormuz towards the west, NW-SE-trending fault zones dominate the area (as shown in Fig. 1 and 2b). These faults are part of the ZMFS complex which has the same direction as the Zagros Orogeny. The ZMFS complex cuts through the trend of the accretionary prism, indicating that it is younger than the onshore part of the prism. To strengthen the results, automated lineament analysis applied to existing onshore geological maps (Fig. 4a). The area was divided into three domains: western, central, and eastern (Fig. 4b). Lineament orientation was analyzed by generating rose diagrams for each of the domains. The results reveal two main dominant directions for each lineament set (Fig. 4c). An E–W trend, perpendicular to plate convergence across the Makran accretionary prism; and a secondary set that varies from NE–SW in the western domain, to nearly E–W in the central domain, and SW–NE in the eastern domain (Fig. 4c). Comparing the lineaments orientation with the geological age of outcrops indicates that, in younger geological units, lineaments tend to be oriented more towards the ENE direction. In contrast, older units predominantly exhibit lineaments with N-S or NW-SE orientations. We note that the eastern boundary of the Makran subduction zone in Pakistan is defined by the Chaman Fault, a major right-lateral plate boundary structure (e.g., *Lawton et al.*, 2008; Szeliga et al.*,* 2010). Stress transfer from this large strike-slip system may influence fault orientations and lineament trends in the eastern part of the Iranian Makran, but its effect on the western Makran and ZMFS is limited.

In the western domain of the Oman Sea, offshore seismic profiles (this study; Pajang et al., 2021, 2022; Kukowski et al., 2001) reveal several steeply dipping fault planes, most of which strike approximately N–S to NE–SW. The fault segments appear discontinuous and subparallel, with little evidence of linkage into large-scale flower structures. Although the raw seismic lines were initially displayed with a vertical exaggeration of 1:5, which can distort the apparent dip of faults, depth converted line and fault interpretation was subsequently carried out at a 1:1 vertical exaggeration to preserve true dip angles (Figs. 5 and 6). Under these corrected conditions, many faults dip between 65° and 85°, rather than appearing near vertical.

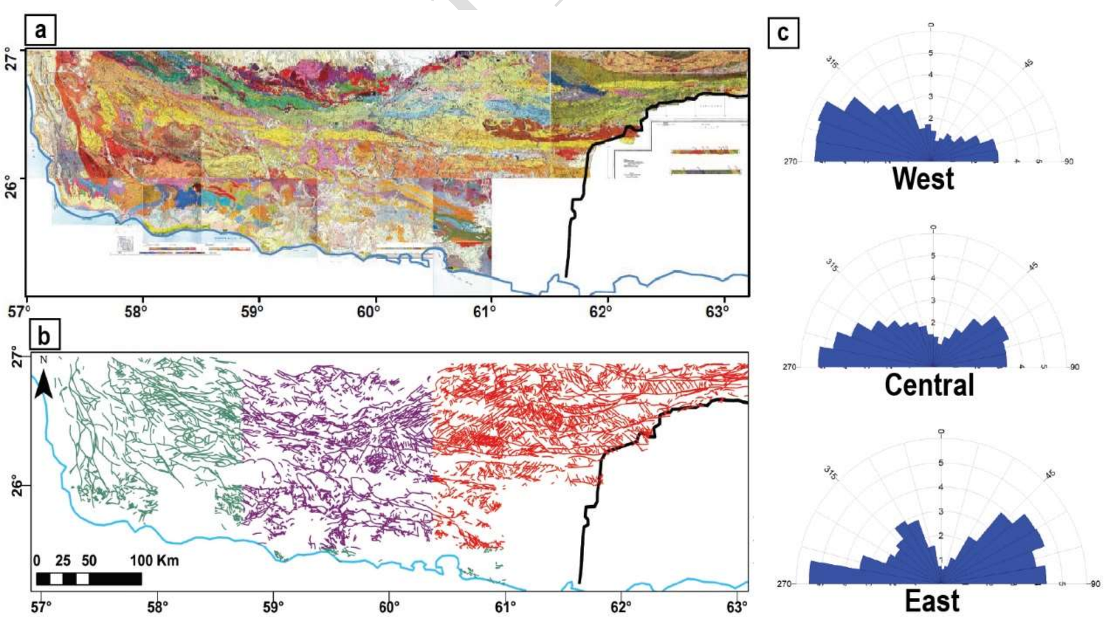

Figure 4. (a) Published geological map of the onshore Iranian part of the Makran zone. The 1:100,000-scale geological maps of Jask, Gabric, Pveshk, Zarabad, Bandini, Kahir, Pirsohrab, and Chabahar cover the coastal area, while the remaining area is represented by 1:250,000-scale maps of Taherui, Fannuj, Nikshahr, and Pishin. (b) Lineaments extracted from geological maps. (c) Rose diagrams showing the trend of lineaments derived from geological maps and satellite images

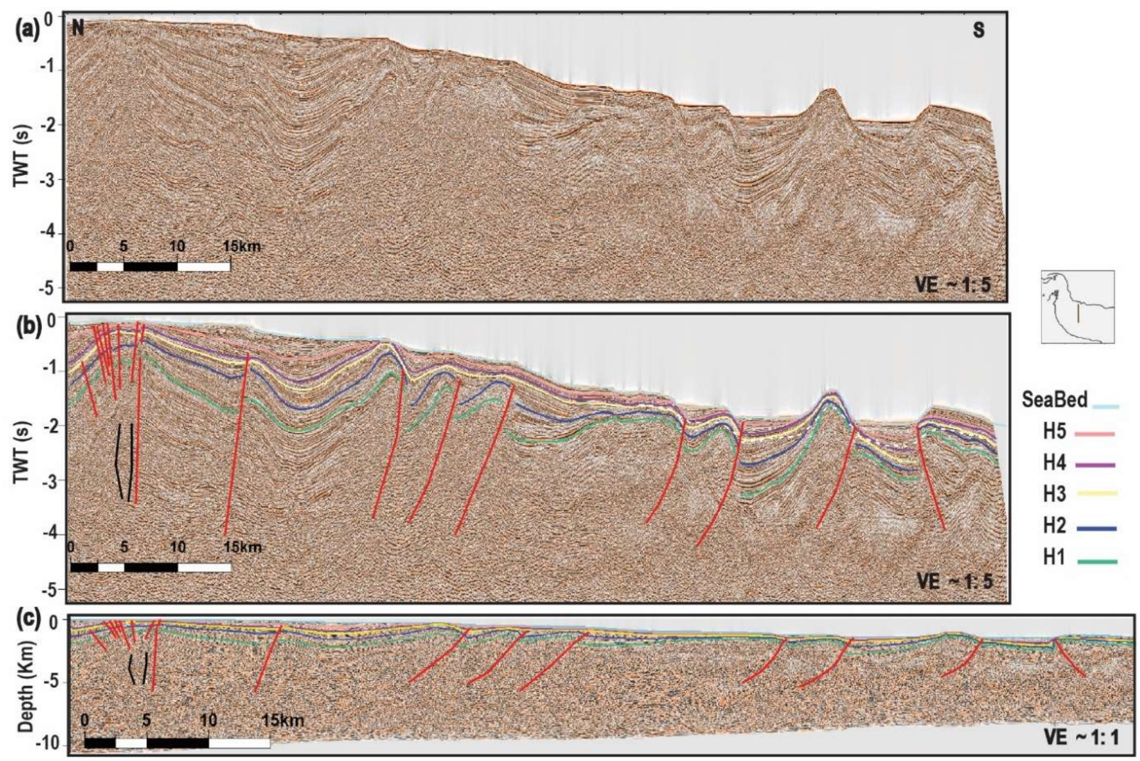

Figure 5. (a) Uninterpreted and (b) interpreted 2D dip seismic line from the western Oman Sea, with its location shown in Figure 2a. Mud volcanoes are outlined by black lines, and faults are marked in red. The bottom-simulating reflector (BSR) is indicated by a white dashed line. The upper panel shows the time-migrated seismic section with vertical exaggeration (VE) ≈ 1:5, and (c) the lower panel presents the depth-converted interpreted section displayed at VE = 1:1

From north to south, fault strikes gradually rotate from N–S near the coast to more E–W in deeper offshore domains. Correspondingly, dips also vary from steep (near vertical) to moderately inclined (toward the NE). Some strike-slip–like faults transition southward into thrusts that merge with the accretionary wedge.

Seismic data interpretation

Using the N–S inline seismic profile shown in Figure 2, the closest 20-s recorded line is the western profile of Pajang et al. (2021). According to their interpretation, this ~97 km-long section does not extend to the trench (Fig. 2c). Water depth increases southward, reaching ~1700 m. The section is characterized by a seaward-dipping active listric normal fault likely rooted in the décollement, a shallow-origin shale diapiric zone, and an imbricated thrust system at the wedge front (Pajang et al., 2021). Approximately 60 km farther west, the N–S seismic line shown in Figure 5 runs parallel to this profile (see Fig. 2 for locations). Although this line also does not reach the frontal thrust, the wedge structure is well defined, consisting of a basal décollement, mud diapir, imbricate thrusts, and shallow splay faults that form seafloor-cored anticlines. Radial normal faults at the toe indicate gravitational collapse of the outer wedge, while vertically disrupted reflectors and chimneys mark zones of fluid escape and elevated pore pressure within the sediment pile. The dashed white line marks a Bottom Simulating Reflector (BSR), caused by minor free gas accumulations beneath the gas hydrate layer, cutting across seismic reflectors and running parallel to the seabed. The active faults are identified from evidence including tilting of recent sediments, fanning geometries, wedge-shaped growth packages, and fault tips that reach the seabed. Farther west, into the Musandam slope (Fig. 6), a large rollover structure is visible, clearly postdating the pre-Tertiary unconformity (dashed black line). The rollover is associated with thickness changes in the Tertiary succession and is detached from the relatively undeformed pre-Tertiary basement.

To better understand the structure in the area, we also present a series of the crossline seismic sections running west-east of the study area (Figs. 7 and 8, location 2a). They reveal piggyback basins with rollover geometries and syn-tectonic growth packages consistent with gravitational normal faulting on a weak décollement horizon. Duplex-like, small-scale thrusts occur locally above mechanically weak, high pore-pressure zones are interpreted as local duplexes formed where newly deposited, low-density sediments act as décollement layers. Several vertical to subvertical features reach the seafloor and produce dome-shaped morphologies; where these are bounded by drag folding rather than planar offsets they are interpreted as potential diapirs or mud-volcano conduits rather than pure faults. Transparent seismic facies above some of these features suggest ongoing fluid or sediment mobilization. Mud diapirs are outlined with black lines. Where their continuation is uncertain either due to interference from surrounding diapirs or the limited seismic resolution they are shown with dashed black lines. Fault segments are largely discontinuous and subparallel, with limited evidence for through-going flower structures. The central portion of the line is characterized by disrupted and attenuated reflectors consistent with mud diapirism or mass-transport complexes, whereas the trenchward domain shows imbricated thrusting consistent with the Makran accretionary complex.

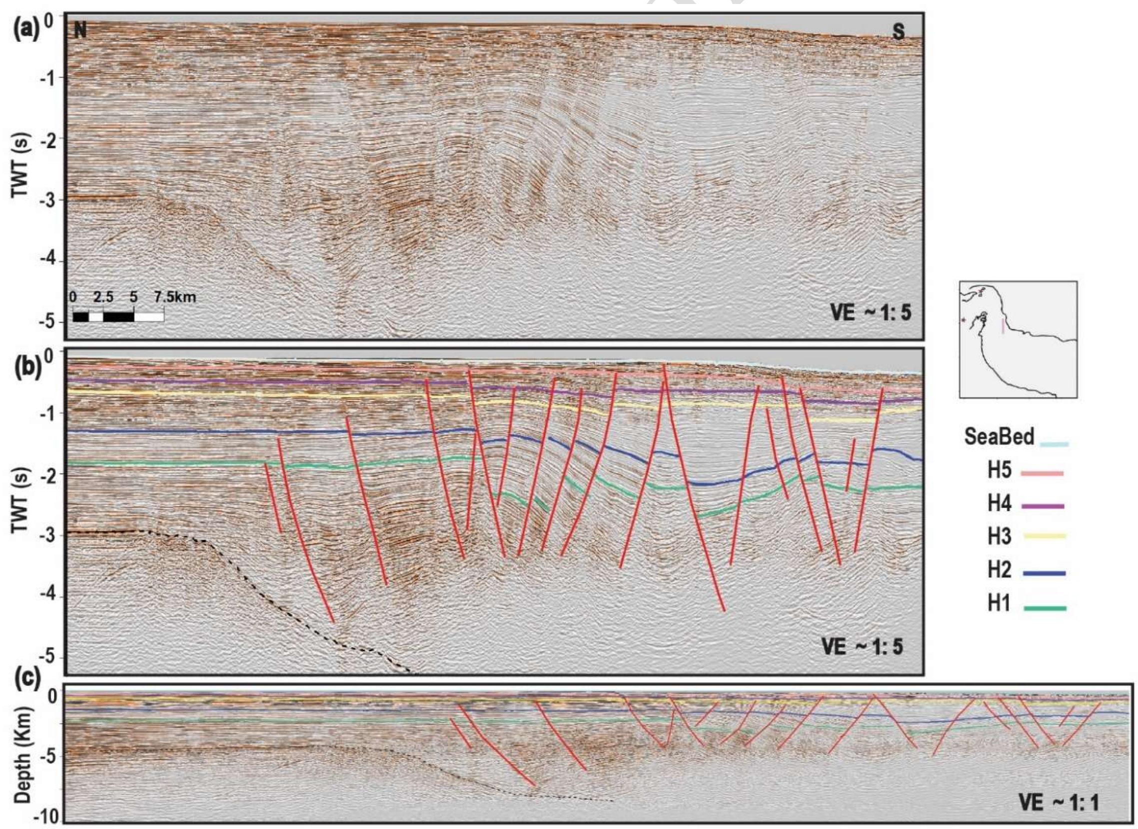

Figure 6. (a) Uninterpreted and (b) interpreted 2D dip seismic line across the Musandam Slope, with its location shown in Figure 2a. The section illustrates a rollover structure on the Musandam Slope. The upper panel shows the time-migrated seismic section with a vertical exaggeration (VE) ≈ 1:5, and (c) the lower panel presents the depth-converted interpreted section displayed at VE = 1:1

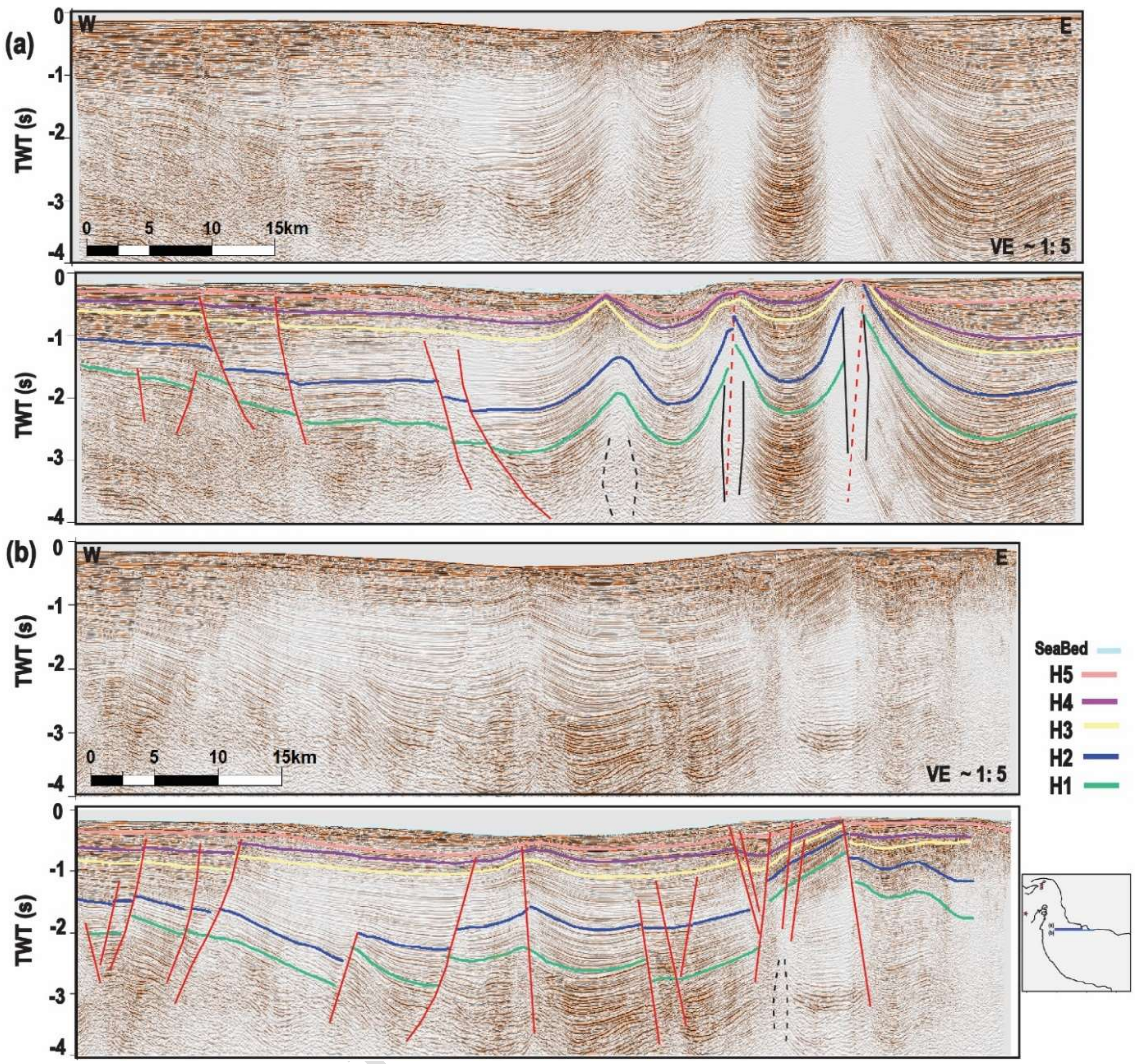

Figure 7. Uninterpreted and interpreted west–east-oriented 2D strike seismic lines from the western Oman Sea illustrate the key structural and stratigraphic features of the subsurface. Their locations are shown in Figure 2a. Mud volcanoes and faults are indicated by black and red lines, respectively. Uncertain interpretations are represented by dashed lines

It is important to note the poor seismic imaging over large areas of the western Oman Sea affected by complex geology, and several interpretations (in particular, attribution of certain domes to diapirs versus fault terminations) remain tentative because the dataset is limited to ~4 s two-way time. The overall geometry demonstrates active shortening, wedge growth, and ongoing fluid migration, consistent with previous descriptions of the Makran prism. Toward the western Oman Sea, however, the structures become steeper and more complex, reflecting the along-strike transition from typical subduction-related accretion to a transpressional regime associated with the offshore continuation of the Zagros–Makran transfer system.

Horizon maps description

Time and depth converted maps of the horizons are shown in Figure 9. The water depth varies significantly within the study area from 0 m at the coastline to more than 1800 m to the south. Low relief topography indicates a calm tectonic regime in the shallow water domain, whereas high relief shows active tectonics in the thrust belt and accreted mélange zone (Fig. 9, Seabed).

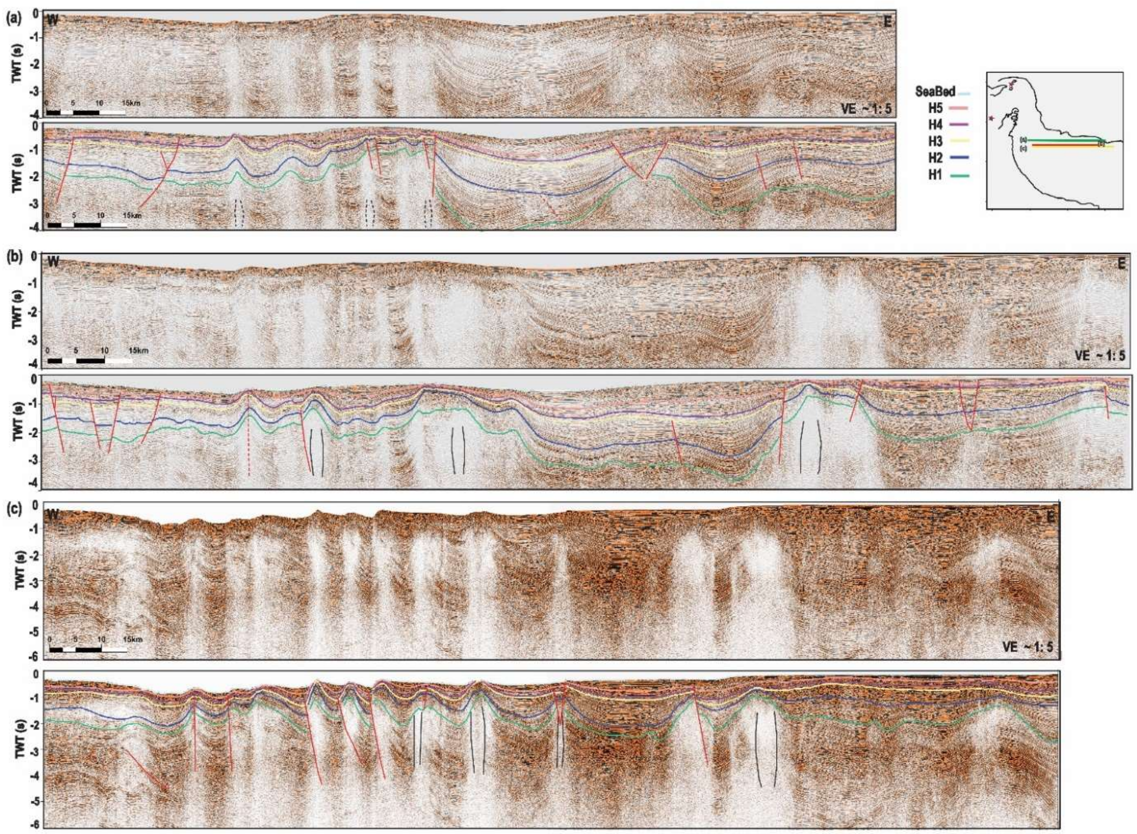

Figure 8. 2D strike-seismic lines of west Oman sea, through the offshore Zendan-Minab Fault Complex, its location shown in Figure 2a. The black lines indicate the mud volcanoes, and the red lines show the faults

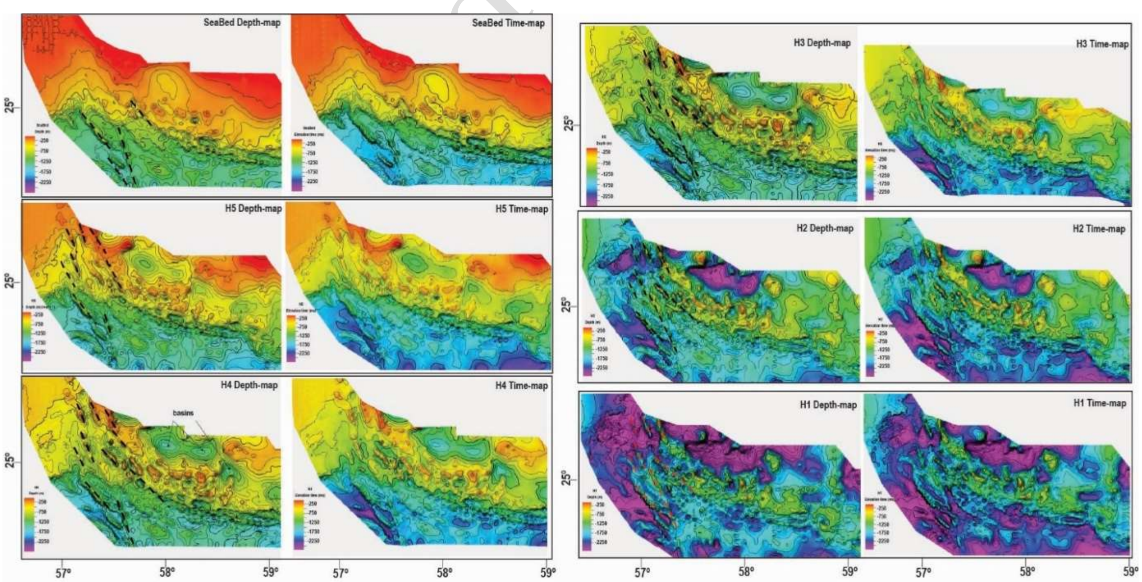

Figure 9. Time- and depth-converted horizon maps. The dashed lines represent lineation trends on different horizon surface maps, potentially indicating strike-slip faults associated with the ZMFS. Note that some of the identified offshore faults, particularly those trending east–west, may also exhibit thrust fault components. The domes are mostly associated with mud diapirism and fluid migration, while the sub-basins are related to normal fault activity in the coastal area

The H5 horizon, a shallow unconformity, shows a regional southward deepening, consistent with the prism dip toward the trench, but is locally disrupted by fault-bounded highs and subcircular features interpreted as mud volcanoes. Along the coast, basins display thickening sequences in response to listric faulting (Fig. 9, H5–H4), and several mud diapirs are observed north of the Accreted Mélange Zone.

The isochore map between the seabed and H4 highlights basin development along the coast, where sediment thickness increases northward. This thickening occurs on the footwall side of listric normal faults bounding the northern margins of half-grabens, emphasizing their role in accommodating basin formation and differential subsidence. In contrast, overburden thickness in the southern part of the area does not exceed 600 m. Several closures are present at this level, mainly associated with diapirs and the thrust belt in the deepest water domain.

The Musandam domain dips eastward, with overburden thickness increasing in that direction, despite the present-day flat seabed. This geometry likely reflects flexure of the Arabian Plate beneath the Eurasian Plate during oblique collision, which created space for sediment accumulation.

Several closures have been identified on the depth map for the H3, H2 and H1 horizons (Fig. 9), most of which fault-related. Increasing depth to the north results from sub-basins formed by listric faulting, whereas overburden generally thins toward the south, approaching the Accreted Mélange Zone. A central high area is observed between a set of transfer faults.

Edge-detection results

By knowing the general trend of the ZMFS on 2D seismic lines, we applied edge detection techniques to horizon depth-converted maps to delineate the offshore extension of the ZMFS (Fig. 10). Edge detection, an image processing method that identifies edges by detecting discontinuities in brightness, provides an efficient and accurate tool for fault interpretation. It enables automatic fault tracking, facilitates rapid and reliable seismic reconstruction, reduces geological interpretation uncertainty, and allows the extraction of fault patches to accelerate the interpretation workflow, thereby supporting a confident and validated structural framework of the subsurface.

The edge-detection results for the H5 and H1 horizons (Fig. 10) reveal systematic variations in structural expression with depth that reflect the offshore continuation of the ZMFS. The H5 horizon exhibits relatively subdued edge responses, particularly in the northern and central sectors, indicating smoother topography and limited deformation within the coastal basin. Only a few weak, NE–SW-trending linear features are observed, interpreted as the shallow expression and possibly strike-slip faults related to the ZMFS. Their subdued appearance likely results from thick sediment cover and reduced relief at these shallow structural levels.

In contrast, the deeper H1 horizon displays a denser and more continuous pattern of linear and curvilinear edges, especially toward the central and southern parts of the area. These edges delineate fault-bounded highs, thrust-related ridges, and zones of intense deformation within the accreted mélange and thrust belt. The dominant NE–SW-oriented lineaments correspond well with the regional trend of the ZMFS, suggesting that the system extends offshore as a segmented strike-slip zone, locally reactivated under transpressional stress. Subcircular anomalies observed in the H1 horizon coincide with diapiric and fluid-migration features, indicating vertical migration along fault-controlled conduits.

Overall, the increase in fault-related edge intensity from H5 to H1 implies that deformation intensifies with depth, consistent with the transition from a relatively undeformed basin in the north to an actively deforming accretionary domain in the south. The persistence of NE–SW-trending discontinuities across multiple horizons supports the interpretation that the ZMFS continues offshore, where it accommodates oblique convergence between the Arabian and

Eurasian plates through combined strike-slip and compressional movements. The persistence of major edge trends from H5 to H1 supports the interpretation of long-lived, through-going faults that accommodated differential subsidence and basin development.

Discussion

Structural Interpretation and Deformation Style

Seismic studies indicate that sediment thickness near the Makran coastline exceeds 10 km (White, 1982; Harms et al., 1984; Kopp et al., 2000; Burg, 2018), providing a significant fluid source for the accretionary prism (Smith et al., 2014). The main décollement occurs at 3–4 km depth near the deformation front (Fig. 2c; Pajang et al., 2021, 2022). Sediments are partly folded and thrusted above the décollement (White, 1982; Harms et al., 1984; Grando and McClay, 2007; Ellouz-Zimmermann et al., 2007) and partly subducted down to the coastline (Platt and Leggett, 1986; Kopp et al., 2000).

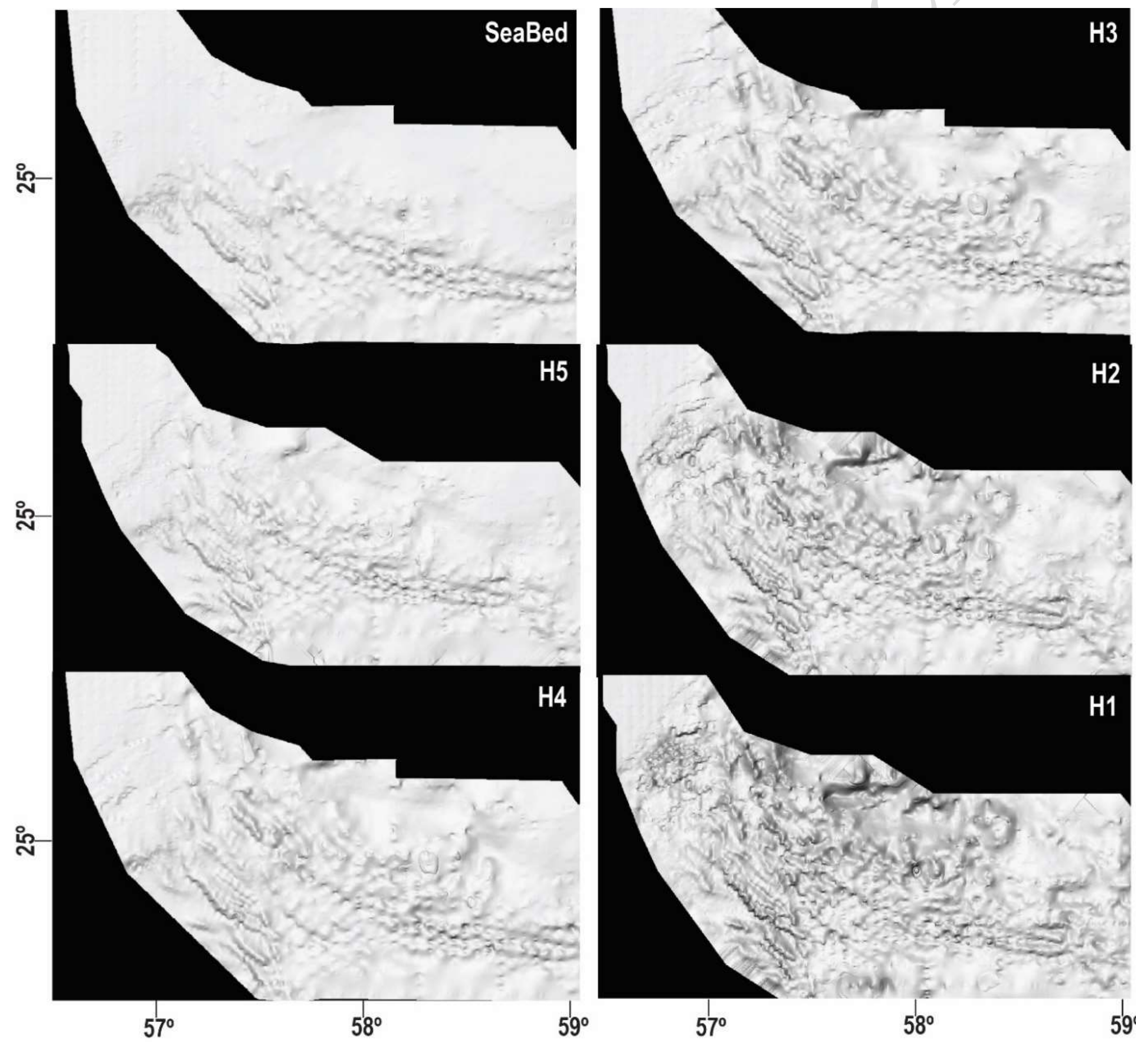

Figure 10. Horizon maps result from edge detection technique to highlight lineaments indicative of fault structures. The lineaments detected on each horizon help to trace the geometry and spatial continuity of faults offshore, allowing for identification of fault trends and possible connections between segments

The Makran prism represents a hybrid system, driven primarily by plate convergence with a minor gravitational component (Yang et al., 2020). High sedimentation promotes upward propagation of normal faults while inhibiting thrust propagation, resulting in distributed deformation. Depth-migrated profiles reveal that deformation offshore combines thrusting and right-lateral strike-slip faulting, with fault dips varying from <25° in the frontal prism to >50° near the coast (Fig. 5). Linear and en-échelon fault segments (Fig. 1) correspond to right-lateral kinematics inferred from GPS data (Abbassi et al., 2023).

Most faults appear geometrically parallel and lack continuous connections, consistent with soft-linked behavior, where segments interact through distributed deformation zones rather than discrete, continuous planes. In contrast, hard-linked structures, such as flower faults, would require clear connections across multiple seismic lines, which cannot be fully resolved given the current 4 × 4 km 2D seismic grid. We note that this grid spacing imposes a limitation on resolving continuous fault traces, and the observed soft-linked appearance may partly reflect this spatial resolution. This diffuse deformation mirrors the onshore ZMFS, where steep right-lateral faults dissect older thrusts and folds (Regard et al., 2010; Mokhtari et al., 2008). The structural trend continues offshore, with fault strikes rotate from N–S to E–W north to south, and dips change from near-vertical to NE-dipping, reflecting the gradual incorporation of right-lateral wrench faults into the wedge. Rose-diagram analysis confirms alignment of offshore faults with the onshore ZMFS.

Dome-shaped structures, mud volcanoes, and fluid chimneys are spatially associated with fault intersections, indicating that faults serve as conduits for overpressured fluids. Some domes with drag folding likely represent mud diapirs, while hybrid structures along pre-existing strike-slip faults are also plausible (Minshull and White, 1989; Kopp et al., 2000; Kukowski et al., 2001; Schlüter et al., 2002; Babadi et al., 2019). Widespread Bottom Simulating Reflectors (BSRs) highlight continuous fluid migration and its association with folded and faulted structures (Smith et al., 2014).

Tectonic and Geodynamic Implications

The offshore ZMFS acts as a lithospheric-scale transfer zone linking the Zagros collision with the Makran subduction system. GPS data indicate ~16 mm yr^{-1} of right-lateral motion along the onshore ZMFS, with part of the strain likely accommodated offshore (Abbassi et al., 2023). Steep strike-slip faults interacting with thrusts and diapirs form a broad transpressional corridor, analogous to other oblique convergent margins such as Sumatra–Andaman and Nankai (Tanioka et al., 1997; Strasser et al., 2009). The offshore ZMFS likely functions as a tear fault or lateral ramp, accommodating differential coupling between western and eastern Makran segments.

High sedimentation generates overpressured, low-density sediments that promote ductile behavior, gravitational gliding, and local duplex formation (Pajang et al., 2021). Fluid-assisted deformation facilitates soft-linked fault interactions, controlling both strain partitioning and the pathways of sediment and fluid migration (Smith et al., 2014; Yang et al., 2020).

Seismotectonic Significance

Although instrumental seismicity is low, structural and geodetic evidence indicates ongoing strain accumulation. Intersections of strike-slip and thrust segments offshore may host moderate to large earthquakes. GPS coupling models show partial interseismic locking along the coast (Abbassi et al., 2023), consistent with episodic elastic strain release. The 2013 Mw 6.1 Minab earthquake demonstrates that intraplate strike-slip faults in the transition zone can generate significant rupture (Penney et al., 2015), and offshore faults may present similar seismic and tsunamigenic potential.

Hence, the offshore ZMFS represents a key, previously underrecognized seismogenic structure transferring strain between the Zagros collision and Makran subduction systems. These observations underscore the need for targeted 3D seismic surveys and marine geodesy to constrain slip rates, fault segmentation, and coupling behavior along this critical Arabia–Eurasia plate boundary transition.

Interpretations presented here are limited by the 2D seismic grid spacing, variable vertical exaggeration, and absence of well control. Fault dips and linkage patterns should be viewed as first-order approximations. Future work integrating 3D seismic, high-resolution bathymetry, and well data would enable more robust assessment of fault kinematics, fluid systems, and geohazard potential.

Conclusion

This systematic change in lineament orientation with decreasing age suggests a progressive lateral eastward migration of active faulting over time. (Fig. 4).

Integration of 2D seismic reflection data, GPS velocities, and published seismicity reveals that deformation in the western Makran is partitioned between thrusting and right-lateral strike-slip faulting, reflecting the offshore continuation of the Zendan–Minab Fault System (ZMFS) (Fig. 11).

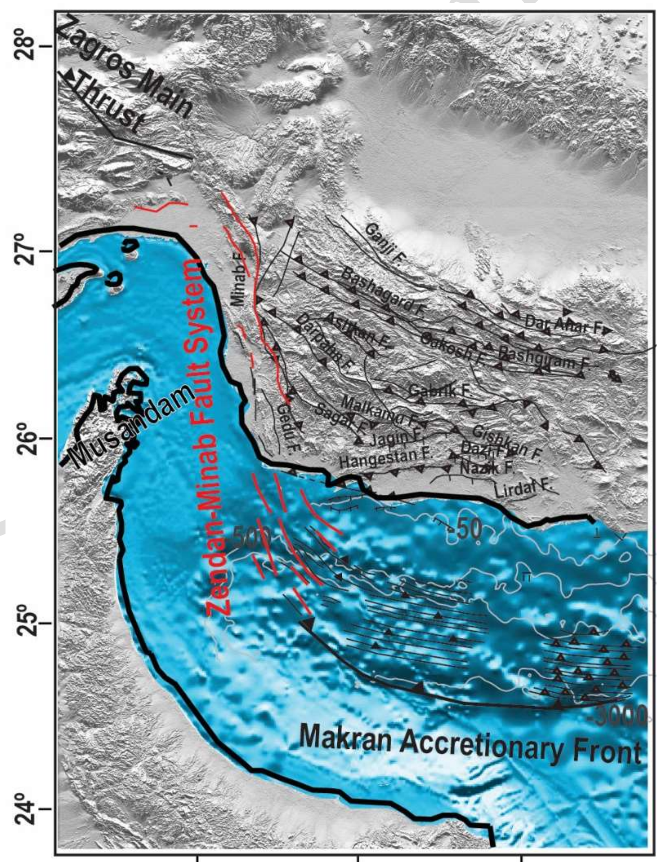

Figure 11. Map of the offshore extension of the ZMFS. The black-colored faults are sourced from existing literature and geological maps, while the red faults represent those confirmed or obtained through the findings of this study. Imbricate thrust faults offshore from (Pajang et al., 2021)

The offshore structural framework consists of three main domains; (i) a coastal extensional zone dominated by listric normal faults; (ii) a central diapiric belt characterized by mud volcanism, fluid migration pathways, and disrupted reflectors; and (iii) a frontal imbricate thrust zone forming the active deformation front. This zonation records a progressive transition from transpression near the coast to compression toward the trench, consistent with oblique convergence between the Arabian and Eurasian plates.

Faults appear soft-linked rather than continuous, indicating distributed shear and fault segmentation typical of oblique convergent margins. We acknowledge that the 2D seismic grid spacing (4×4 km) imposes constraints on resolving continuous fault planes. Therefore, the observed “soft-linked” appearance could partly result from spatial resolution, rather than solely tectonic processes. Measured fault dips ($<25°$ to $>50°$) and the gradual rotation of fault orientations from north–south to east–west likely reflect strain partitioning associated with the tectonic transition from the Zagros–Makran transfer zone (collision regime) toward the Makran subduction zone, where deformation becomes increasingly thrust-dominated.

The offshore ZMFS functions as a lithospheric-scale transfer fault that accommodates differential motion between the Zagros collision and Makran subduction systems. GPS-derived rates (~16 mm yr^{-1} of right-lateral motion) imply that a significant portion of the strain is transferred offshore, where it is absorbed by a broad, transpressional fault corridor. The interaction between steep strike-slip faults, thrusts, and diapiric structures suggests that fluid overpressure and high sedimentation rates (>10 km) promote ductile deformation, local duplexing, and gravitational gliding within the upper wedge.
Although western Makran exhibits relatively low seismicity, geodetic coupling models and structural evidence indicate ongoing strain accumulation along the ZMFS and associated offshore faults. Moderate to large earthquakes could occur where strike-slip and thrust systems intersect, with potential tsunamigenic implications.

Author Contributions

Mehrdad Sarhangi (Data curation: Lead; Formal analysis: Lead; Software: Lead; Visualization: Lead; Writing original draft: Lead; Writing review & editing: Lead)
Ali Solgi (Methodology: Equal; Supervision: Equal; Validation: Equal; Writing original draft: Equal; Writing review & editing: Equal)
Morteza Talebian (Methodology: Equal; Supervision: Equal; Validation: Equal; Writing original draft: Equal; Writing review & editing: Equal)
Zahra Maleki (Supervision: Equal; Validation: Equal; Writing original draft: Equal; Writing review & editing: Equal)

Conflicts of interest

The authors declare no conflict of interest

References

Abbasi, M., Ghods, A., Najafi, M., Abbasy, S., Amiri, M., Shabanian, E., Asgari, J. 2023. Why does western Makran have a low seismicity rate? Tectonophysics, 869, 230134.
Ahmed, S. S. 1969. Tertiary geology of part of south Makran, Baluchistan, West Pakistan. AAPG Bulletin, 53, 1480–1499.
Alavi, M. 1994. Tectonics of the Zagros orogenic belt of Iran: New data and interpretations. Tectonophysics, 229, 211–238.
Allen, M. B., & Armstrong, H. A. 2008. Arabia–Eurasia collision and the forcing of mid-

Cenozoic global cooling. Palaeogeography, Palaeoclimatology, Palaeoecology, 265, 52–58.
Aram, Z. & Arian, M. 2016. Active Tectonics of the Gharasu River Basin in Zagros, Iran, Investigated by Calculation of Geomorphic Indices and Group Decision Using Analytic Hierarchy Process (AHP) Software. Episodes, 39, 39-44.
Babadi, M. F., Mehrabi, B., Tassi, F., Cabassi, J., Vaselli, O., Shakeri, A., Pecchioni, E., Venturi, S., Zelenski, M., & Chaplygin, I. 2019. Origin of fluids discharged from mud volcanoes in SE Iran. Marine and Petroleum Geology, 106, 190–205.
Bayer, R., Chéry, J., Tatar, M., Vernant, P., Abbassi, M., Masson, F., Nilforoushan, F., Doerflinger, E., Regard, V., & Bellier, O. 2006. Active deformation in Zagros–Makran transition zone inferred from GPS measurements. Geophysical Journal International, 165, 373–381.
Burberry, C., & Jackson, C. 2013. Structural development of the western Makran accretionary complex, offshore Iran. In AGU Fall Meeting Abstracts (pp. T41E–04).
Burg, J. P. 2018. Geology of the onshore Makran accretionary wedge: Synthesis and tectonic interpretation. Earth-Science Reviews, 185, 1210–1231.
Burg, J. P., Bernoulli, D., Smit, J., Dolati, A., & Bahroudi, A. 2008. A giant catastrophic mud-and-debris flow in the Miocene Makran. Terra Nova, 20, 188–193.
Casini, G., Gillespie, P., Vergés, J., Romaire, I., Fernández, N., Casciello, E., Saura, E., Mehl, C., Homke, S., & Embry, J. C. 2011. Sub-seismic fractures in foreland fold and thrust belts: Insight from the Lurestan Province, Zagros Mountains, Iran. Petroleum Geoscience.
Chiu, H. Y., Chung, S. L., Zarrinkoub, M. H., Mohammadi, S. S., Khatib, M. M., & Iizuka, Y. 2013. Zircon U–Pb age constraints from Iran on the magmatic evolution related to Neotethyan subduction and Zagros orogeny. Lithos, 162, 70–87.
Ellouz-Zimmermann, N., Deville, E., Müller, C., Lallemant, S., Subhani, A., & Tabreez, A. 2007. Impact of sedimentation on convergent margin tectonics: Example of the Makran accretionary prism (Pakistan). In Thrust Belts and Foreland Basins (pp. 327–350). Springer.
Frohling, E., & Szeliga, W. 2016. GPS constraints on interplate locking within the Makran subduction zone. Geophysical Supplements to the Monthly Notices of the Royal Astronomical Society, 205, 67–76.
Geological Survey of Iran. (n.d.). Geological Map of Taherui, Fannuj, Nikshahr and Pishin, 1:250,000 series. Tehran: Geological Survey of Iran.
Geological Survey of Iran. (n.d.). Geological Map of Jask, Gabric, Pveshk, Zarabad, Bandini, Kahir, Pirsohrab and Chabahar, 1:100,000 series. Tehran: Geological Survey of Iran.
Ghods, A., Bergman, E., Aghdam, M. A., Khaledzadeh, M., & Enayat, M. 2025. Geodynamics of the Makran subduction zone inferred from relocated seismicity. Tectonophysics, 905, 230716.
Grando, G., & McClay, K. 2007. Morphotectonic domains and structural styles in the Makran accretionary prism, offshore Iran. Sedimentary Geology, 196, 157–179.
Haberland, C., Mokhtari, M., Babaei, H. A., Ryberg, T., Masoodi, M., Partabian, A., & Lauterjung, J. 2020. Anatomy of a crustal-scale accretionary complex: Insights from deep seismic sounding of the onshore western Makran subduction zone, Iran. Geology, 49, 3–7.
Harding, T. P. 1985. Seismic characteristics and identification of negative flower structures, positive flower structures, and positive structural inversion. AAPG Bulletin, 69, 582–600.
Harms, J., Cappel, H., & Francis, D. 1984. The Makran coast of Pakistan: Its stratigraphy and hydrocarbon potential. Marine Geology and Oceanography of the Arabian Sea and Coastal Pakistan, 3, 27.
Hessami, K., Koyi, H., & Talbot, C. J. 2001. The significance of strike-slip faulting in the basement of the Zagros fold and thrust belt. Journal of Petroleum Geology, 24, 5–28.
Kadinsky-Cade, K., & Barazangi, M. 1982. Seismotectonics of southern Iran: The Oman Line. Tectonics, 1, 389–412.

Khaledzadeh, M., & Ghods, A. 2023. Along-strike segmentation of seismogenic zone in the offshore Makran megathrust zone as revealed by seafloor bathymetry and free-air gravity anomalies. SSRN Electronic Journal.

Khorrami, F., Vernant, P., Masson, F., Nilforoushan, F., Mousavi, Z., Nankali, H., Saadat, S. A., Walpersdorf, A. S., Tavakoli, P., Aghamohammadi, A., & Alijanzade, M. 2019. An up-to-date crustal deformation map of Iran using integrated campaign-mode and permanent GPS velocities. Geophysical Journal International, 217, 832–843.

Kopp, C., Fruehn, J., Flueh, E., Reichert, C., Kukowski, N., Bialas, J., & Klaeschen, D. 2000. Structure of the Makran subduction zone from wide-angle and reflection seismic data. Tectonophysics, 329, 171–191.

Kukowski, N., Schillhorn, T., Huhn, K., von Rad, U., Husen, S., & Flueh, E. R. 2001. Morphotectonics and mechanics of the central Makran accretionary wedge off Pakistan. Marine Geology, 173, 1–19.

Masson, F., Anvari, M., Djamour, Y., Walpersdorf, A., Tavakoli, F., Daignières, M., Nankali, H., & Van Gorp, S. 2007. Large-scale velocity field and strain tensor in Iran inferred from GPS measurements. Geophysical Journal International, 170, 436–440.

McCall, J., Rosen, B., & Darrell, J. 1994. Carbonate deposition in accretionary prism settings: Early Miocene coral limestones and corals of the Makran Mountain Range in southern Iran. Facies, 31, 141–177.

McClay, K., & Bonora, M. 2001. Analog models of restraining stepovers in strike-slip fault systems. AAPG Bulletin, 85, 233–260.

McQuarrie, N., Stock, J., Verdel, C., & Wernicke, B. 2003. Cenozoic evolution of Neotethys and implications for the causes of plate motions. Geophysical Research Letters, 30.

Minshull, T., & White, R. 1989. Sediment compaction and fluid migration in the Makran accretionary prism. Journal of Geophysical Research: Solid Earth, 94, 7387–7402.

Mokhtari, M., Abdollahie Fard, I., & Hessami, K. 2008. Structural elements of the Makran region, Oman Sea, and their potential relevance to tsunamigenesis. Natural Hazards, 47, 185–199.

Mohammadi, A., Burg, J. P., Winkler, W., Ruh, J., & von Quadt, A. 2016. Detrital zircon and provenance analysis of Late Cretaceous–Miocene onshore Iranian Makran strata: Implications for the tectonic setting. Bulletin, 128(9-10), 1481-1499.

Mohammadi, A., Burg, J. P., Guillong, M., & von Quadt, A. 2017. Arc magmatism witnessed by detrital zircon U-Pb geochronology, Hf isotopes and provenance analysis of Late Cretaceous-Miocene sandstones of onshore western Makran (SE Iran). American Journal of Science, 317(8), 941-964.

Moody, J. D., & Hill, M. J. 1956. Wrench-fault tectonics. Geological Society of America Bulletin, 67, 1207–1246.

Namdarsehat, P., Milczarek, W., Motavalli-Anbaran, S. H., & Khaledzadeh, M. 2024. Makran subduction zone: A review and synthesis. Geosciences, 14(8), 219.

Pajang, S., Cubas, N., Letouzey, J., Le Pourhiet, L., Seyedali, S., Fournier, M., Agard, P., Khatib, M. M., Heyhat, M., & Mokhtari, M. 2021. Seismic hazard of the western Makran subduction zone: Insight from mechanical modelling and inferred frictional properties. Earth and Planetary Science Letters, 562, 116789.

Pajang, S., Khatib, M. M., Heyhat, M., Cubas, N., Bessiere, E., Letouzey, J., Mokhtari, M., & Le Pourhiet, L. 2022. The distinct morphologic signature of underplating and seamounts in accretionary prisms: Insights from thermomechanical modeling applied to coastal Iranian Makran. Tectonophysics, 845, 229617.

Penney, C., Copley, A., & Oveisi, B. 2015. Subduction tractions and vertical axis rotations in the Zagros–Makran transition zone, SE Iran: The 2013 May 11 Mw 6.1 Minab earthquake. Geophysical Journal International, 202, 1122–1136.

Penney, C., Tavakoli, F., Saadat, A., Nankali, H. R., Sedighi, M., Khorrami, F., Sobouti, F., Rafi, Z., Copley, A., & Jackson, J. 2017. Megathrust and accretionary wedge properties and behaviour in the Makran subduction zone. Geophysical Journal International, 209, 1800–1830.
Peyret, M., Djamour, Y., Hessami, K., Regard, V., Bellier, O., Vernant, P., Daignières, M., Nankali, H., & Van Gorp, S. 2009. Present-day strain distribution across the Minab–Zendan–Palami fault system from dense GPS transects. Geophysical Journal International, 179, 751–762.
Platt, J. P., & Leggett, J. K. 1986. Stratal extension in thrust footwalls, Makran accretionary prism: Implications for thrust tectonics. AAPG Bulletin, 70, 191–203.
Ravaut, P., Carbon, D., Ritz, J. F., Bayer, R., & Philip, H. 1998. The Sohar Basin, western Gulf of Oman: Description and mechanisms of formation from seismic and gravity data. Marine and Petroleum Geology, 15, 359–377.
Regard, V., Bellier, O., Thomas, J. C., Abbassi, M., Mercier, J., Shabanian, E., Feghhi, K., & Soleymani, S. 2004. Accommodation of Arabia–Eurasia convergence in the Zagros–Makran transfer zone, SE Iran. Tectonics, 23, TC4007.
Regard, V., Bellier, O., Thomas, J. C., Bourlès, D., Bonnet, S., Abbassi, M., Braucher, R., Mercier, J., Shabanian, E., & Soleymani, S. 2005. Cumulative right-lateral fault slip rate across the Zagros–Makran transfer zone: Role of the Minab–Zendan fault system. Geophysical Journal International, 162, 177–203.
Regard, V., Leturmy, P., Mouthereau, F., Mercier, J.-L., & Mohajer-Ashjai, A. 2008. Tectonic evolution of the Zendan–Minab fault zone and Makran accretionary prism (SE Iran): Implications for the Arabia–Eurasia convergence. Tectonophysics, 449, 123–142.
Regard, V., Mouthereau, F., Leturmy, P., Mercier, J.-L., & Mohajer-Ashjai, A. 2009. Kinematics and deformation partitioning in the Makran accretionary prism and Zendan–Minab fault zone (SE Iran). Journal of Structural Geology, 31, 383–400.
Regard, V., Hatzfeld, D., Molinaro, M., Aubourg, C., Bayer, R., Bellier, O., Yamini-Fard, F., Peyret, M., & Abbassi, M. 2010. The transition between Makran subduction and the Zagros collision: Recent advances in its structure and active deformation. Geological Society, London, Special Publications, 330, 43–64.
Ricou, L. E. 1977. Le croissant ophiolitique péri-arabe, une ceinture de nappes mises en place au Crétacé supérieur. Revue de Géographie Physique et de Géologie Dynamique, 19, 327–350.
Ruh, J. B., Vergés, J., & Burg, J. P. 2018. Shale-related minibasins atop a massive olistostrome in an active accretionary wedge setting: Two-dimensional numerical modeling applied to the Iranian Makran. Geology, 46, 791–794.
Schlüter, H., Prexl, A., Gaedicke, C., Roeser, H., Reichert, C., Meyer, H., & Von Daniels, C. 2002. The Makran accretionary wedge: Sediment thicknesses and ages and the origin of mud volcanoes. Marine Geology, 185, 219–232.
Smith, G., McNeill, L., Henstock, T. J., & Bull, J. 2012. The structure and fault activity of the Makran accretionary prism. Journal of Geophysical Research: Solid Earth, 117, B07406.
Smith, G. L., McNeill, L. C., Henstock, T. J., Arraiz, D., & Spiess, V. 2014. Fluid generation and distribution in the highest sediment input accretionary margin, the Makran. Earth and Planetary Science Letters, 403, 131–143.
Stoneley, R. 1981. The geology of the Kuh-e Dalneshin area of southern Iran, and its bearing on the evolution of southern Tethys. Journal of the Geological Society, 138, 509–526.
Swanson, M. T. 2005. Geometry and kinematics of adhesive wear in brittle strike-slip fault zones. Journal of Structural Geology, 27(5), 871–887.
Talbot, C., & Alavi, M. 1996. The past of a future syntaxis across the Zagros. Geological Society, London, Special Publications, 100, 89–109.

Tanioka, Y., Ruff, L., & Satake, K. 1997. What controls the lateral variation of large earthquake occurrence along the Japan Trench? Island Arc, 6(3), 261–266.
Vernant, P., Nilforoushan, F., Hatzfeld, D., Abbassi, M., Vigny, C., Masson, F., Nankali, H., Martinod, J., Ashtiani, A., & Bayer, R. 2004. Present-day crustal deformation and plate kinematics in the Middle East constrained by GPS measurements in Iran and northern Oman. Geophysical Journal International, 157, 381–398.
Walker, R., & Jackson, J. 2002. Offset and evolution of the Gowk fault, SE Iran: A major intracontinental strike-slip system. Journal of Structural Geology, 24, 1677–1698.
Walpersdorf, A., Hatzfeld, D., Nankali, H., Tavakoli, F., Nilforoushan, F., Tatar, M., Vernant, P., Chéry, J., & Masson, F. 2006. Difference in the GPS deformation pattern of north and central Zagros (Iran). Geophysical Journal International, 167, 1077–1088.
White, R. S. 1982. Deformation of the Makran accretionary sediment prism in the Gulf of Oman (north-west Indian Ocean). Geological Society, London, Special Publications, 10, 357–372.
Yamini-Fard, F., Hatzfeld, D., Mokhtari, M., & Farahbod, A. 2003. Microseismicity and crustal structure of the transition zone Zagros–Makran based on the data of a local dense temporary seismological network. In Fourth International Conference of Earthquake Engineering and Seismology (pp. 1–6). Tehran, Iran.
Yang, X., Peel, F. J., McNeill, L. C., & Sanderson, D. J. 2020. Comparison of fold–thrust belts driven by plate convergence and gravitational failure. Earth-Science Reviews, 206, 103136.
Zalan, P. V. 1987. Identification of strike-slip faults in seismic sections. In SEG Technical Program Expanded Abstracts 1987 (pp. 116–118). Society of Exploration Geophysicists.